Third International Conference on Sustainable Construction Materials and Technologies http://www.claisse.info/Proceedings.htm

An Experimental Study on Corrosion Protection Performance of HPFRCCs with Fine Cracks

Le Anh Dung[1], Koichi Kobayashi[2], Keitetsu Rokugo[3]

[123]*Department of Civil Engineering, Gifu University, Yanagido 1-1, Gifu 501-1193, Japan*
[1]*r3121026@edu.gifu-u.ac.jp*, [2]*ko2ba@gifu-u.ac.jp*, [3]*rk@gifu-u.ac.jp*

ABSTRACT

This paper regards the application of HPFRCC as a patching repair material. In order to ensure tensile strain-hardening property and to improve workability, the replacement of cement by limestone powder, and the decrease of fiber content in HPFRCC mix were examined. The conclusions are as follows: As the fiber content decreased, the ultimate strain of HPFRCC decreased, whereas the tensile strength and compressive strength had no evident change and the average crack width was almost identical. Reducing the fiber content to 0.75% and replacing of Portland cement by limestone powder did not affect the corrosion preventing performance of HPFRCC while the workability was improved.

Keywords. HPFRCC, Chloride penetration, Rebar corrosion, Patch repair

INTRODUCTION

High performance fiber reinforced cement composite (HPFRCC), is considered to be suitable for a patching repair material thanks to its strain hardening and multiple fine crack behavior under tensile stress. In our research, it was clearly observed that HPFRCC have high impermeability to chloride because the crack width being very small (Kobayashi, 2010).

However, in order to develop HPFRCC as a patching repair material, high toughness is not necessary in performance of HPFRCC, while high corrosion protection performance and fine workability is importance. Therefore, the corrosion protect performance of HPFRCC, containing the low fiber contents, are yet to be clarified.

To achieve such properties concurrently, the replacement of cement by limestone powder, and the decrease of fiber content in HPFRCC mix were examined. The chloride penetration depth and corrosion proofing performance were investigated to develop a HPFRCC mixture to be suitable for a patching repair material.

MECHANICAL PERFORMANCE OF HPFRCC

Materials and mixtures. The mix proportions of HPFRCC are shown in Table 1. The fiber used in this study was the PE fiber with a length of 12 mm, a diameter of 0.0012 mm and the tensile strength of 2.6 GPa. The cement used was a high early strength Portland cement. The silica sand had a diameter ranged from 100 to 200µm. The volume fractions of fiber were 1.5, 1.0, and 0.75 % to compare the influence of fiber content on performance of HPFRCC. Mixture A has been used as a standard mixture in our previous studies, and is used as a reference in this study. Mixture B had a lower fiber content in comparison with mixture A. In order to improve the workability furthermore, Cement in the mixtures C and D was replaced by limestone powder. In these two mixtures, the percentage of limestone powder replacement was 45% by mass. Mixture E is a pre-packed material that is commercially available. This mixture contains fly ash as a part of binder, and used both PE and PVA fibers.

Table 1. Mixture compositions of HPFRCC

Mix	W/C (%)	Unit mass (kg/m^3)						
		W	C	Limestone powder	Silica sand	HRWRA	VA	Fiber
A	30	380	1264	-	395	18.96	0.9	14.6(1.5vol%)
B	30	385	1280	-	400	19.2	0.91	7.3(0.75vol%)
C	40	360	900	300	462	13.5	0.63	9.7(1.0vol%)
D	40	340	850	283	595	12.75	0.6	7.3(0.75vol%)

Mix	W/B	S/B	Unit mass (kg/m^3)						
			W	B	Silica sand	Polymer	HRWRA (powder)	Fiber (1.9vol%)	
								PE	PVA
E	28.5	31.9	328	1149	367	37	4.4	6	15.8

Uniaxial tension test. The uniaxial tension tests were carried out on dumbbell-shaped specimens (JSCE, 2008).

After the tensile test, the number and width of cracks that were generated in the guage length of 80 mm, were measured by using the microscope with 50x magnification. The crack width was measured for one specimen which was the nearest to the average tensile strain of five specimens. The localized crack, showing the largest crack width, was excluded.

Properties of HPFRCC. The mortar flow of HPFRCC mixtures are shown in Table 2. Mixture B with 0.75% PE fiber had lower flow value than mixture A with 1.5% fiber. The decreasing fiber content result in the increased table flow, leaded to better fiber dispersion, improved workability of HPFRCC. The replacement of Portland cement by limestone powder causes a decrease in the compressive strength that can be explained as a result of cement dilution effect. The influences of PE fiber content on compressive strength of HPFRCC were not clearly observed.

The cracking strength, the tensile strength and the ultimate strain are also shown in Table 2. After the first cracking, the specimens were not broken, the stress increased as the strain increased, showing the strain-hardening behavior was clearly observed in all the HPFRCC mixtures. However, the reduction of PE fiber at mixtures B and D result in the low ductility of HPFRCC, whereas there was no evident change in the tensile strength.

The replacement of limestone powder results in the decrease in the tensile strength of the matrix, reflected by the decrease in the first cracking strength as shown in Table 2. The decreased matrix strength leads to the high ductility of the HPFRCC composite (Zhou, 2009).

Table 2. Flow and mechanical performance of HPFRCC

Mix	Mortar flow(mm)		Mechanical properties							
			Compressive strength (MPa)	Tension test			Cracks			
	Before table drop	After table drop		First craking strength	Tensile strength (MPa)	Ultimate strain (%)	Number of cracks	Crack width (mm)		
								Average	Min	Max
A	132	158	80.5	5.11	8.37	3.46	65	0.025	0.014	0.046
B	168	191	83.0	4.52	5.96	0.50	5	0.027	0.014	0.042
C	149	178	63.4	4.20	5.86	0.91	12	0.023	0.014	0.041
D	154	184	68.8	4.17	6.09	0.24	3	0.022	0.014	0.026
E	133	170	52.2	4.91	6.65	5.28	60	0.020	0.012	0.051

Cracks in HPFRCC. The number of cracks and the average crack width are also shown in Table 2. The increasing PE fiber content results in the increased number of cracks. Mixtures B and D with 0.75% fiber had little number of cracks than another mixture with higher fiber content. The ultimate strain shows a strong relation with the number of cracks as shown in Figure 1. The higher ultimate strain gives the matrix more chances to crack.

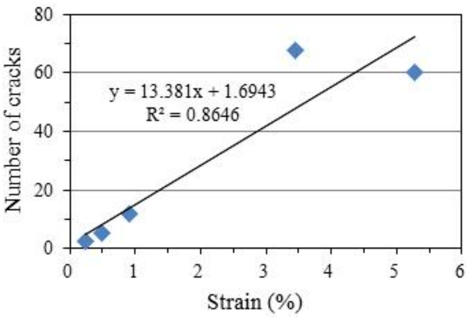

Figure 1. Relationship between strain and number of cracks

All mixtures show the average of crack width range of from 0.02 to 0.027 mm. And the maximum crack width was 0.051mm. Mixtures A-D with the same type of fiber results in that the average crack width was almost identical, and that 90% of cracks width range from 0.02 to 0.04 mm. In mixture E, 60% of crack width ranges from 0.02 to 0.03mm.

CORROSION PROTECTION BY HPFRCC

Materials and mix proportions. Normal concrete (NC) with a W/C of 0.55 was used as the base material, and HPFRCC was used as a patching repair material. NC exhibits a compressive strength of 46.9MPa, a slump value of 16 cm, and an air content of 4.7%. The mixtures of HPFRCC are the same as those shown in Table 2.

Specimens. In this study, 2 types of specimens were used to investigate the corrosion protection performance of HPFRCC – monolithic specimen and patched specimen. Patched specimens simulate a patch repair using HPFRCC to restore a cross section of RC member to the backside of the reinforcing bars. As shown in Figure 2, RC beam size was 100 mm in width, and 1700 mm in length. A threaded D25 bar was welded to two D10 bars 1500 mm in length at each end.

The monolithic specimen size was 50 mm in depth. The patched specimen size was 80 mm in depth. HPFRCC were overlaid by shotcreting to a thickness of 40 mm over pairs D10 rebars arranged on the beams of NC with a cross section of 40 mm × 100 mm. The mortar on the substrate NC surface was washed away by water on the next day of casting to simulate removal of deteriorated surface concrete by high-pressure water jet. After demolding, all beams (total in 11) were cured with wet burlap for about one month. The method of introduction of cracks into the beam was shown in Figure 2. The threaded D25 bars were pulled by using a center-hole hydraulic jack in a unixial direction. Cracking on the surfaces was visually observed, and the crack width was measured by microscope with 50x magnification.

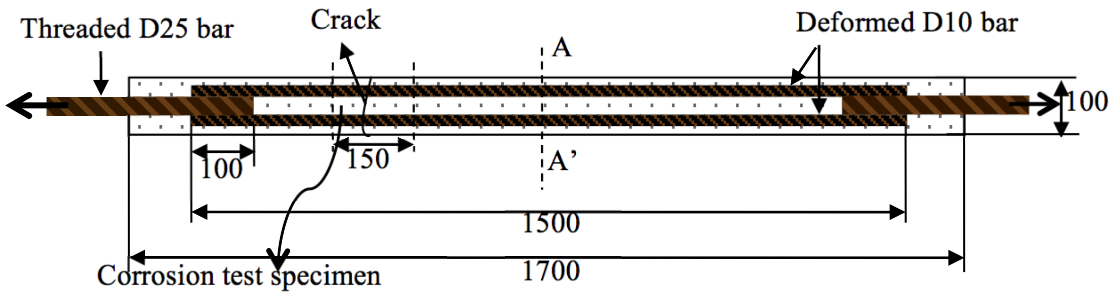

Figure 2. Method of generating cracks in the beam (unit: mm)

Repeated loading was applied while progressively increasing the load until the crack with in the substrace NC part reached 0.5 mm in the monothilic NC beam and the double-layer beams, or 0.03 mm in the monothilic HPFRCC beams.

After introducing cracks, two specimens with length of 150 mm were cutted out from the cracked parts of the beams to be used in the penetration tests. 150mm long specimens are shown in Figure 3. And then, the crack width in the upper side of specimens were measured by microscope. Five sides of the specimens were then sealed by epoxy paint so that the chloride can penetrate only in one-direction.

Measurement of chloride penetration depth and steel corrosion. Immediately after sealing, all specimens was set chamber to be sprayed by 3% NaCl solution for 5 min every 6 hours in order to accelerate the deterioration. After 150 days of chloride spraying, all specimens were taken out from the chamber to measure chloride penetration depth.

To measure chloride penetration depth, the specimens were split open, and then sprayed with 0.1 N silver nitrate ($AgNO_3$) solution on fresh surfaces. After measuring the chloride penetration depth, the reinforcing bars were taken out from the specimens. The corroded parts on the reinforcing bar was traced on a OHP film to measure the corrosion area using a parameter.

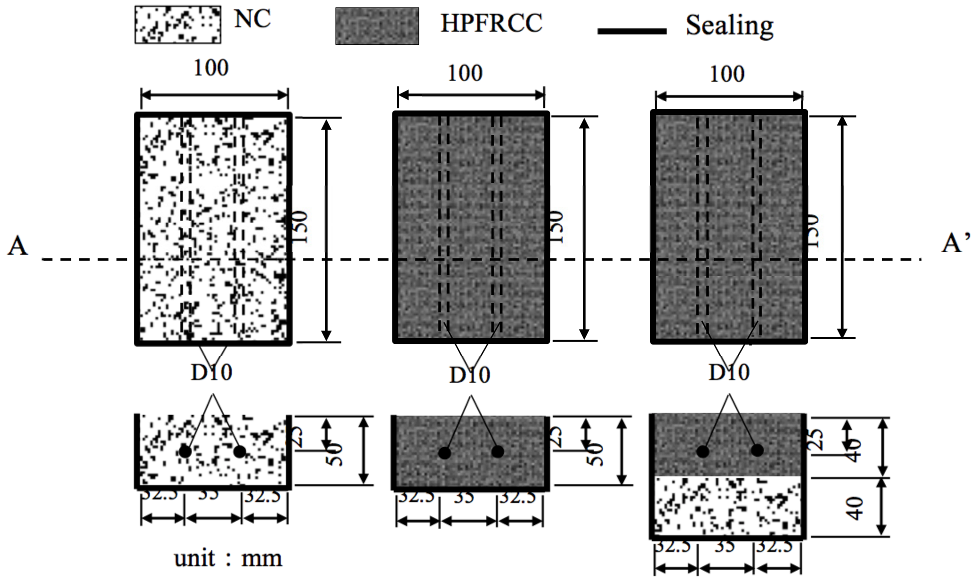

a) NC monolithic b) HPFRCC monolithic c) HPFRCC patched

Figure 3. Corrosion test specimens

Table 4. Crack properties and penetration depth

Specimens	Crack width (mm)				Number of crack(s)	Chloride penetration depth(mm)
	NC substrate	HPFRCC				
		Average	Total	Maximum		
Monolithic specimens						
A-1	-	0.020	0.326	0.032	16	13
A-2	-	0.032	0.664	0.055	21	25
B-1	-	0.028	0.611	0.051	22	16
B-2	-	0.020	0.139	0.031	7	8
C-1	-	0.033	0.394	0.104	12	23
C-2	-	0.023	0.346	0.041	15	16
D-1	-	0.025	0.300	0.037	12	11
D-2	-	0.023	0.114	0.032	5	24
E-1	-	0.024	0.120	0.041	5	4
E-2	-	0.022	0.179	0.031	8	11
NC-1	0.249	-	—	0.496	3	50
NC-2	0.196	-	—	0.523	3	50
Patched specimens						
A-1	0.880	0.021	0.063	0.023	3	9
A-2	0.308	0.000	0.000	0	0	8
B-1	0.037	0.031	0.153	0.041	5	10
B-2	0.113	0.018	0.054	0.02	3	10
C-1	0.645	0.020	0.102	0.031	5	12
C-2	0.502	0.028	0.085	0.031	3	19
D-1	0.262	0.027	0.080	0.037	3	20
D-2	0.420	0.024	0.094	0.031	4	22
E-1	0.379	0.031	0.031	0.031	1	7
E-2	0.563	0.019	0.037	0.023	2	7

Crack distribution. Table 4 shows the crack width and number of cracks in both the substrate part and the repair part. HPFRCC mixtures show the average of crack widths range from 0.020 to 0.033 mm.

A large crack runs transversely throughout the monolithic NC specimens. However, multiple fine cracks were generated in the monolithic HPFRCC specimens. In the patched specimens, while only one large crack was generated in the NC substrate part, the HPFRCC part had multiple fine cracks spearing from the point where the large crack in the NC substrate part reached the surface between the NC part and HPFRCC part (Figure 4). This characteristic was observed in all patched specimens. Therefore, crack distribution proves a fine bond between HPFRCC and NC. The influence of fiber content on the crack distributions were not clear in two types of the specimens that used HPFRCC.

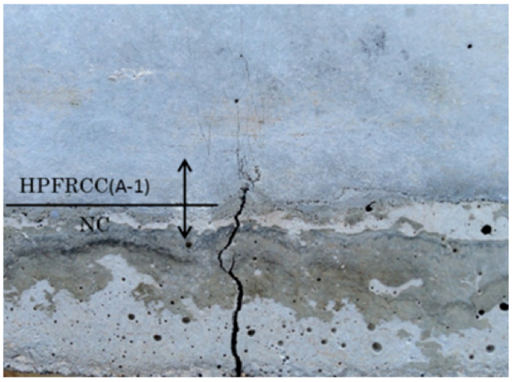

Figure 4. Example of cracks in the patching specimen A-1

Chloride penetration. Figure 5 shows examples of the results of the chloride penetration test. Figure 6 shows the chloride penetration depth in specimens. The red line in this figure shows the location of the D10 bars.

In the case of monolithic NC specimens, chloride penetration concentrates where the pre-crack was located as shown in Figure 5(b), and chloride had reached up to the bottom surface. In the case of monolithic HPFRCC specimens, the penetration depth was shallow, and the chloride had not reached up to the location of D10 bars with the exception of the A-2 monolithic specimen. In another words, chloride penetration depth in HPFRCC mixtures was lower than that of the NC mixture. The crack width HPFRCC specimen was smaller than 0.05 mm, so the chloride penetration rates were very lower than that of NC specimens with large crack width of 0.2mm (Wang, 1997). It can be said therefore that HPFRCC with micro-cracks exhibited a much increased chloride penetration resistance than NC.

In the case of patched specimens, the chloride had not reached up to the bond between HPFRCC part and NC part. It was observed that the HPFRCC repaired part with 40 mm depth was able to prevent chloride penetration. The penetration depths of chloride in mixtures A and B were shallower than those of mixtures C and D. This may be caused by the low water-binder ratio.

The influence of PE fiber content on the penetration depth of chloride was not observed in both types of the specimens.

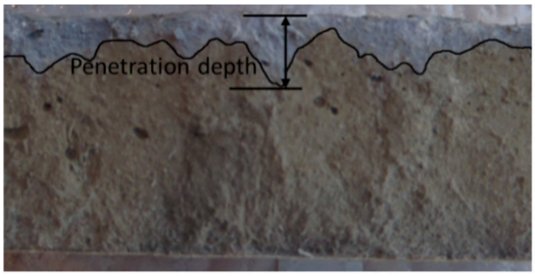

(a) A-1 Monolithic specimen

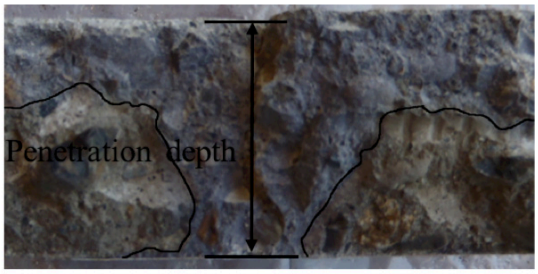

(b) NC-1 Monolithic specimen

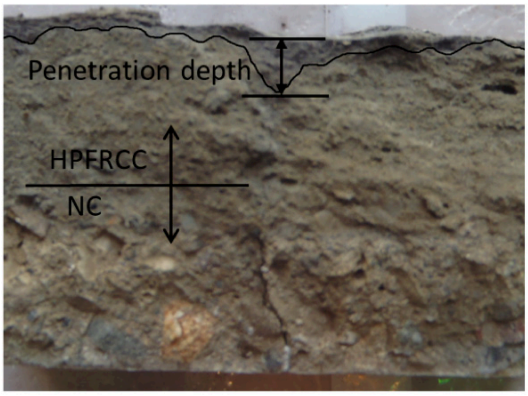

(c) A-1 Patched specimen

Figure 5. Examples of chloride penetration

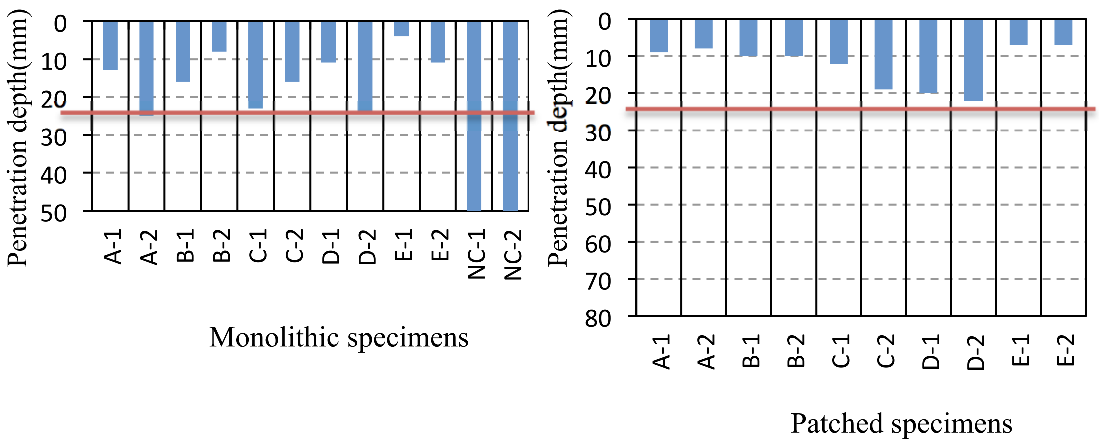

Figure 6. Chloride penetration depth in specimens

Figure 7 shows the relationship between the crack width and the penetration depth. It was observed that the influence of each value of crack width (the maximum and the total crack width) on the penetration depth had the same trend. In the case of mixtures A and B, the crack width shows a strong relation with penetration depth of chloride in monolithic specimens. However, all the patched specimens with mixtures A and B, the crack width had

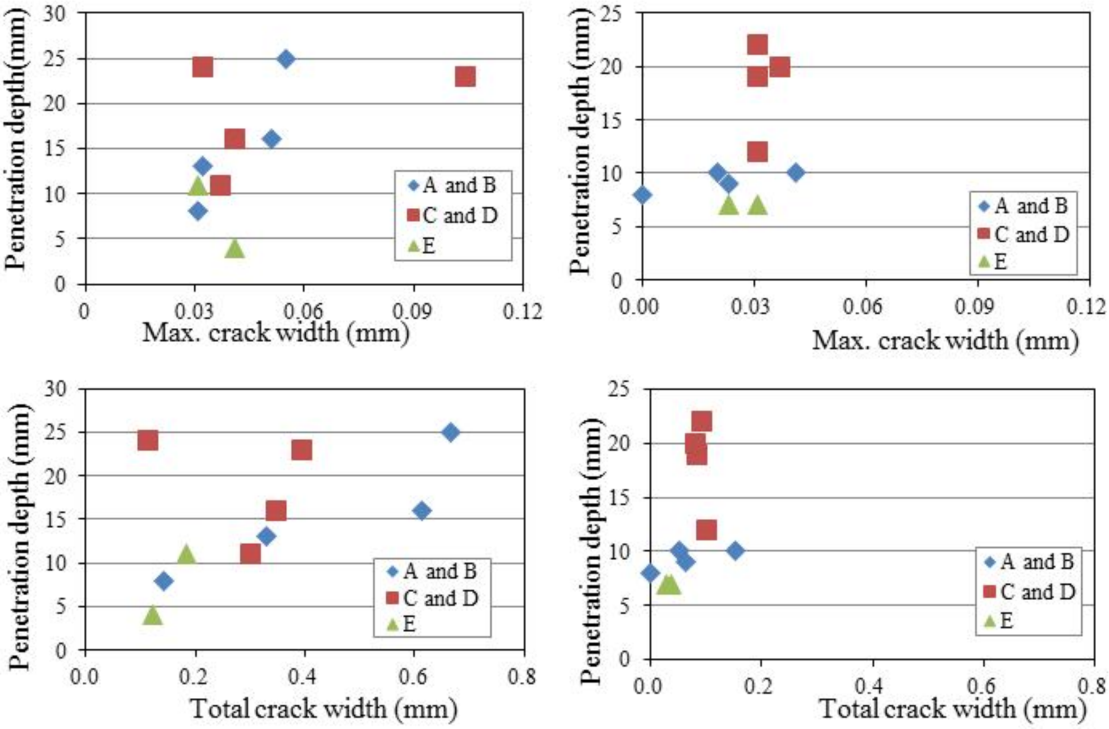

(a) Monolithic specimens (b) Patched specimens

Figure 7. Relationship between cracks and penetration depth

the same chloride penetration depth regardless of the crack width. The reason for this is a little number of cracks generated in HPFRCC side of patched specimens. In case of mixtures C and D, the relationship between the crack width and the penetration depth was not observed in both the monolithic and patched specimens.

Corrosion of rein forcing bar. Table 5 shows the ratio of corrosion area on the reinforcing bars. The reinforcing bars did not corrode in all the monolithic HPFRCC specimens and patched specimens with the exception of the E-1 patched specimen. The generation of fine multiple crack is caused by a smaller fracture area between the matrix and the steel. In addition, the low water cement ratio of HPFRCC decreases, the quantity of

Table 5. Corrosion area ratio on two steel rebars

Specimens	Corrosion area(cm^2)		Corrosion area ratio (%)	
	bar 1	bar 2	bar 1	bar 2
Monolithic specimens				
NC -1	16.6	16.6	35.3	35.3
NC -2	15.8	14.8	33.5	31.5
Patched specimens				
E -1	15.6	-	33.2	-

oxygen permeation, resulting in the slowed corrosion rate slows down.

CONCLUSIONS

In this study, the applicability of HPFRCC as a patching repair material was investigated. To achieve such properties concurrently, the replacement of cement by limestone powder, and the decrease of fiber content in HPFRCC mix were examined. The chloride penetration depth and corrosion proofing performance were investigated to develop a HPFRCC mixture to be suitable for a patching repair material. The conclusions are as follows:

(1) As the fiber content decreased, the ultimate strain decreased, whereas the tensile strength and compressive strength had no evident change.

(2) The decreased fiber content lead to a decreased number of cracks, while the average crack width was almost identical.

(3)HPFRCC with micro-cracks exhibited a much increased chloride penetration resistance than NC.

(4)Reducing the fiber content to 0.75% and replacing of Portland cement by limestone powder did not affect the corrosion preventing performance of HPFRCC while improved workability.

REFERENCES

JSCE Concrete Committee. (2008) Recommendations for design and construction of high performance fiber reinforced cement composites with multiple fine cracks (HPFRCC). Concrete engineering series No. 82.

Kobayashi, K., Iizuka, Y., Kurachi, H., and Rokugo, K. (2010) “Corrosion protection performance of High Performance Fiber Reinforced Cement Composites as a repair material”. Cement & Concrete Composites, 32: 411-420

Wang, K., Jansen, D. C., Shah, S. P. (1997) “Permeability study of cracked concrete. Cement and Concrete Research, 27, 3: 381-393

Zhou, J., Qian, S., Beltran, M. G. S., Ye, G., Breugel, K., and Li, V. C. (2009) “Development of engineered cementitious composites with limestone powder and blast furnace slag”. Materials and Structures 43: 803-814